A Semi-implicit and Unconditionally Stable Approximation of the Surface Tension in Two-phase Fluids

Byungjoon Lee, Gangjoon Yoon and Chohong Min

July 18, 2019

Abstract

We focus on the energy conservation of two-phase fluids, where the change in kinetic energy is balanced by the gravitational potential and the surface energy related to surface tension. We introduce an unconditionally stable approximation in the sense that the total energy does not increase with any time step. An analysis is presented to prove the unconditional stability property of the scheme, and numerical results are given to confirming the analysis.

1 Introduction

The conservation of energy is a prominent law of physics. The motion of a physical object may increase or decrease each particular energy, but keeps the total sum of energies. For example, when a fluid streams down hills, some of the gravitational potential energy is converted into an equal amount of kinetic energy. The energy transfer between gravitational potential and kinetic energy is a fact that is well known and familiar to even non-scientists, but much less known is the transfer between surface energy and kinetic energy, which is the topic of this research.

Consider two immiscible fluids separated by an interface Γ. Surface tension arises on the interface, due to differences in the attraction forces between the molecules of the two fluids [17]. The support of the surface tension is thus the interface, its magnitude is linearly proportional to the mean curvature of the interface, and pointing in the normal direction [18, 21, 6]. Based on these facts, we formulate two-phase fluids by the following system:

$$\rho_t + U \cdot \nabla \rho = 0 \text{ in } \Omega,$$
$$\rho \left(U_t + U \cdot \nabla U \right) = -\nabla p - \rho g e_y - \sigma \kappa n \delta_\Gamma \text{ in } \Omega,$$
$$\nabla \cdot U = 0 \text{ in } \Omega,$$
$$U = 0 \text{ on } \partial \Omega,$$

where Ω represents the computational domain and $\partial \Omega$ its boundary.

When the fluid is inviscid, the above system preserves the total energy, i.e. the sum of the kinetic energy and potential energies [8, 14]. Surface tension turns out to be a factor in minimizing the surface area, and the surface potential energy is defined as the surface area times the parameter $\sigma \in \mathbb{R}$. Potential energies include the gravitational potential and the surface potential. Let us denote by $E(t)$, the total energy of the system at time t:

$$E(t) := \int_\Omega \frac{1}{2} \rho U^2 dV + \int_\Omega \rho g y dV + \rho |\Gamma|$$

Making uses of shape derivatives and material derivatives [15], we obtain the following equation, which states the energy conservation:

$$\frac{dE}{dt} = \int_\Omega \rho U \cdot \frac{DU}{Dt} dV + \int_\Omega \rho g e_y \, dV + \sigma \int_\Gamma \kappa \left(U \cdot n \right) ds$$
$$= \int_\Omega U \cdot \left(-\nabla p \right) dV$$
$$= \int_\Omega \left(\nabla \cdot U \right) p \, dV = 0$$

Due to the nonlinearity and the elliptic constraint, it has remained one of the hardest problems in computational fluid dynamics to solve two-phase fluids with surface tension present. Brackbill et al. [4] analyzed a standard numerical method approximating the surface tension explicitly and obtained a CFL condition of $\Delta t = O\left(\Delta x^{1.5}\right)$. Their analysis assumed very simple and restrictive cases: the domain is infinitely long and the interface is of sinusoidal shape. In general however, the domain domain is bounded and the interface is not of sinusoidal. Yet, that time step restriction has been used in many work [1, 16, 20].

The usual CFL condition of the standard methods [12, 2, 5] dealing with single-phase fluid is $\Delta t = O\left(\Delta x\right)$, and thus the inclusion of surface tension significantly restrict the time step from $O\left(\Delta x^{-1}\right)$ to $O\left(\Delta x^{-1.5}\right)$. For example, taking $\Delta x = \frac{1}{100}$ translate into a simulation that is ten times longer; a serious drawback in practice. There have been several achievements to alleviate the strict CFL condition $\Delta t = O\left(\Delta x^{1.5}\right)$: Sussman et al [19], Hysing [7], and Jarauta et al. [9] have developed numerical methods with a CFL condition of $\Delta t = O\left(\Delta x\right)$. The main strategy that is common in these studies is to treat the surface tension semi-implicitly. As a remarkable attempt, we note the work of Zheng et al. [22] that proposed a fully implicit discretization of the surface tension utilizing hybrid particles. . Numerical tests demonstrated that the CFL condition $\Delta t = O\left(\Delta x^{1.5}\right)$ can indeed be relaxed, but no analysis were proposed to guarantee stability.

The object of this paper is to introduce a semi-implicit approximation of two-phase fluids with surface tension, and mathematically prove that the numerical solution is unconditionally stable in terms of the total sum of the kinetic and the potential energies. To the best of our knowledge, this is the first approximation of surface tension that is proven to be stable. We begin with the description of temporal discretization in Section 2 and introduce spatial discretizations in Section 3. Empirical results in Section 4 validate the analysis, but point out that the associated linear system is very ill-conditioned. In Section 5, we discuss what needs to be done in future work to resolve this drawback, which is beyond the scope of this paper.

2   Time discretization

In this article, we propose a semi-implicit approximation of the time derivatives, and prove that the approximation does not increase the total energy. As in [18, 21, 6], we assume that ρ is piecewise constant away from the interface, and smeared out smoothly in a narrow band of the interface. Therefore ρ can be taken as an approximation of the indicator function of the regions occupied by the fluids, from which we derive the following approximations of geometric terms:

$$\nabla \rho \simeq [\rho]\, n \delta_\Gamma \text{ in } \mathbb{R}^d,$$
$$\nabla \cdot \left(\frac{\nabla \rho}{|\nabla \rho|}\right) \simeq \kappa \qquad \text{on } \Gamma,$$
$$|\Gamma| \simeq \frac{1}{[\rho]} \int_{\mathbb{R}^d} |\nabla \rho|\, dV,$$

where, $[\rho]$ denotes the difference in the two constant densities. As in [13], we adopt a new variable $M := \sqrt{\rho}U$, in order to conveniently represent the kinetic energy by an L^2 integral. Using the conservation of mass, $\frac{D\rho}{Dt} = 0$, and in the above geometric approximations, we reformulate the momentum equation as:

$$\rho \frac{DU}{Dt} = \sqrt{\rho}\frac{DM}{Dt}$$
$$= -\nabla p - \rho g e_y - \frac{\sigma}{[\rho]}\nabla \cdot \left(\frac{\nabla \rho}{|\nabla \rho|}\right)\nabla \rho.$$

The convection term in the momentum equation is nonlinear, so that it has been a usual practice to solve the convection equation first completing the solution of the system [12, 2, 5]. We denote by M^*, the solution of the convection equation. As in [11], we apply a Lax-Wendroff type approximation that conserves the L^2 energy:

$$\frac{\tilde{M}^{n+\frac{1}{2}} - M^n}{\Delta t/2} + U^{n+\frac{1}{2}} \cdot \nabla \tilde{M}^{n+\frac{1}{2}} = 0$$
$$\frac{M^* - M^n}{\Delta t} = \frac{\tilde{M}^{n+\frac{1}{2}} - M^n}{\Delta t/2} \tag{1}$$

Here, $U^{n+\frac{1}{2}}$ is an extrapolated incompressible vector field that is defined as:

$$U^{n+\frac{1}{2}} := U^n + \frac{\Delta t}{2} \frac{U^n - U^{n-1}}{t^n - t^{n-1}}.$$

Lemma 1. *The convection solver of equation (1) conserves the L^2 energy, so that $\|M^*\|_{L^2} = \|M^n\|_{L^2}$, for any $\Delta t > 0$.*

Proof. We repeat the analysis of [11] for the sake of completeness.

$$
\begin{aligned}
\frac{\|M^*\|_{L^2}^2 - \|M^*\|_{L^2}^2}{2\Delta t} &= \int_\Omega \frac{M^* + M^n}{2} \cdot \frac{M^* - M^n}{\Delta t} \, dV \\
&= \int_\Omega \tilde{M}^{n+\frac{1}{2}} \cdot \left[U^{n+\frac{1}{2}} \cdot \nabla \tilde{M}^{n+\frac{1}{2}} \right] dV \ (\because \text{integration by parts}) \\
&= -\int_\Omega \tilde{M}^{n+\frac{1}{2}} \cdot \left[U^{n+\frac{1}{2}} \cdot \nabla \tilde{M}^{n+\frac{1}{2}} \right] dV + \int_\Omega \left| \tilde{M}^{n+\frac{1}{2}} \right|^2 \nabla \cdot U^{n+\frac{1}{2}} \, dV \\
&= -\int_\Omega \tilde{M}^{n+\frac{1}{2}} \cdot \left[U^{n+\frac{1}{2}} \cdot \nabla \tilde{M}^{n+\frac{1}{2}} \right] dV = 0,
\end{aligned}
$$

using the fact that $x = -x$ implies $x = 0$ and the incompressibility condition of $U^{n+\frac{1}{2}}$. $\qquad\square$

Using the solution M^*, we propose the following semi-implicit approximation of the system:

$$\sqrt{\rho^n} \frac{M^{n+1} - M^*}{\Delta t} = -\nabla p^{n+1} - \rho^n g e_y - \frac{\sigma}{[\rho]} \nabla \cdot \left(\frac{\nabla \rho^{n+1}}{\sqrt{|\nabla \rho^n|^2 + \epsilon}} \right) \nabla \rho^n, \tag{2}$$

$$\nabla \cdot \left(\frac{M^{n+1}}{\sqrt{\rho^n}} \right) = 0, \tag{3}$$

$$\frac{\rho^{n+1} - \rho^n}{\Delta t} + \frac{M^{n+1}}{\sqrt{\rho^n}} \cdot \nabla \rho^n = 0. \tag{4}$$

Note that the above approximation is a linear system of equation for the unknowns M^{n+1}, p^{n+1}, and ρ^{n+1}. To prevent the division-by-zero, a small number ϵ was added to the denominator. The total variation is accordingly calculated with ϵ, and we measure the energy of the system as:

$$E_\epsilon (M, \rho) := \int_\Omega \frac{M^2}{2} dV - \int_\Omega \rho g y \, dV + \frac{\sigma}{[\rho]} \int_\Omega \sqrt{|\nabla \rho^n|^2 + \epsilon} \, dV.$$

In the above definition, we used an approximation $|\Gamma| \simeq \frac{\sigma}{[\rho]} \int_\Omega \sqrt{|\nabla \rho^n|^2 + \epsilon} \, dV$. Now, we prove that our proposed approximation is stable in the sense that the sequence generated by the approximation does not increase the energy.

Theorem 1. *(Unconditional stability of the time discretization) Let $\left(M^{n+1}, \rho^{n+1} \right)$ be generated from (M^*, ρ^n) by (2)-(4), and let M^* be generated from M^n and $U^{n+\frac{1}{2}}$ by (1). For any $\Delta t > 0$, we have $E_\epsilon \left(M^{n+1}, \rho^{n+1} \right) \leq E_\epsilon (M^n, \rho^n)$.*

Proof. Let us denote $\langle f, g \rangle$ the L^2 inner-product $\int_\Omega fg \, dV$. As the usual L^2 energy estimate starts from $\langle M, M_t \rangle$, we

consider the following identities:

$$\left\langle M^{n+1}, \frac{M^{n+1} - M^*}{\Delta t} \right\rangle = \left\langle \frac{M^{n+1}}{\sqrt{\rho^n}}, -\nabla p^{n+1} - \rho g \nabla y - \frac{\sigma}{[\rho]} \nabla \cdot \left(\frac{\nabla \rho^{n+1}}{\sqrt{|\nabla \rho^n|^2 + \epsilon}} \right) \nabla \rho^n \right\rangle$$

$$= \left\langle \nabla \cdot \left(\frac{M^{n+1}}{\sqrt{\rho^n}} \right), p^{n+1} \right\rangle + \left\langle \nabla \cdot \left(\frac{M^{n+1}}{\sqrt{\rho^n}} \rho \right), y \right\rangle$$

$$+ \frac{\sigma}{[\rho]} \left\langle -\frac{M^{n+1}}{\sqrt{\rho^n}} \cdot \nabla \rho^n, \nabla \cdot \left(\frac{\nabla \rho^{n+1}}{\sqrt{|\nabla \rho^n|^2 + \epsilon}} \right) \right\rangle$$

$$= 0 - \left\langle \frac{\rho^{n+1} - \rho^n}{\Delta t}, y \right\rangle + \frac{\sigma}{[\rho]} \left\langle \frac{\rho^{n+1} - \rho^n}{\Delta t}, \nabla \cdot \left(\frac{\nabla \rho^{n+1}}{\sqrt{|\nabla \rho^n|^2 + \epsilon}} \right) \right\rangle$$

With the non-slip boundary condition on $\partial \Omega$, $\left(\rho^{n+1} - \rho^n \right) / \Delta t = 0$ on $\partial \Omega$, and the following integration by parts holds:

$$\left\langle \frac{\rho^{n+1} - \rho^n}{\Delta t}, \nabla \cdot \left(\frac{\nabla \rho^{n+1}}{\sqrt{|\nabla \rho^n|^2 + \epsilon}} \right) \right\rangle = -\left\langle \frac{\nabla \rho^{n+1} - \nabla \rho^n}{\Delta t}, \frac{\nabla \rho^{n+1}}{\sqrt{|\nabla \rho^n|^2 + \epsilon}} \right\rangle$$

$$= \int_\Omega \frac{-|\nabla \rho^{n+1}|^2 + \nabla \rho^n \cdot \nabla \rho^{n+1}}{\Delta t \sqrt{|\nabla \rho^n|^2 + \epsilon}} dV$$

Using the following two basic inequalities:

$$-|\boldsymbol{a}|^2 + \boldsymbol{a} \cdot \boldsymbol{b} \leq -|\boldsymbol{a}|^2 - \epsilon + |\boldsymbol{a}| |\boldsymbol{b}| + \epsilon$$

$$= -|\boldsymbol{a}|^2 - \epsilon + \sqrt{|\boldsymbol{a}|^2 |\boldsymbol{b}|^2 + 2 |\boldsymbol{a}| |\boldsymbol{b}| \epsilon + \epsilon^2}$$

$$\leq -|\boldsymbol{a}|^2 - \epsilon + \sqrt{|\boldsymbol{a}|^2 |\boldsymbol{b}|^2 + \left(|\boldsymbol{a}|^2 + |\boldsymbol{b}|^2 \right) \epsilon + \epsilon^2}$$

$$= -|\boldsymbol{a}|^2 - \epsilon + \sqrt{\left(|\boldsymbol{a}|^2 + \epsilon \right) \left(|\boldsymbol{b}|^2 + \epsilon \right)}, \text{ and}$$

$$\frac{-|\boldsymbol{a}|^2 + \boldsymbol{a} \cdot \boldsymbol{b}}{\sqrt{|\boldsymbol{b}|^2 + \epsilon}} \leq \frac{-\left(\sqrt{|\boldsymbol{a}|^2 + \epsilon} \right)^2 + \sqrt{\left(|\boldsymbol{a}|^2 + \epsilon \right) \left(|\boldsymbol{b}|^2 + \epsilon \right)}}{\sqrt{|\boldsymbol{b}|^2 + \epsilon}}$$

$$\leq \frac{+\left(\sqrt{|\boldsymbol{b}|^2 + \epsilon} \right)^2 - \sqrt{\left(|\boldsymbol{a}|^2 + \epsilon \right) \left(|\boldsymbol{b}|^2 + \epsilon \right)}}{\sqrt{|\boldsymbol{b}|^2 + \epsilon}}$$

$$= \sqrt{|\boldsymbol{b}|^2 + \epsilon} - \sqrt{|\boldsymbol{a}|^2 + \epsilon},$$

we obtain:

$$\left\langle M^{n+1}, \frac{M^{n+1} - M^*}{\Delta t} \right\rangle \leq -\left\langle \frac{\rho^{n+1} - \rho^n}{\Delta t}, gy \right\rangle + \frac{\sigma}{[\rho]} \int_\Omega \frac{\sqrt{|\nabla \rho^n|^2 + \epsilon} - \sqrt{|\nabla \rho^{n+1}|^2 + \epsilon}}{\Delta t} dV$$

and

$$\left\|M^{n+1}\right\|^2 + \left\langle \rho^{n+1}, gy \right\rangle + \frac{\sigma}{[\rho]} \int_\Omega \sqrt{\left|\nabla \rho^{n+1}\right|^2 + \epsilon} \, dV \leq \left\langle M^{n+1}, M^* \right\rangle + \left\langle \rho^n, gy \right\rangle + \frac{\sigma}{[\rho]} \int_\Omega \sqrt{\left|\nabla \rho^n\right|^2 + \epsilon} \, dV$$

$$\leq \frac{1}{2}\left\|M^{n+1}\right\|^2 + \frac{1}{2}\left\|M^*\right\|^2 + \left\langle \rho^n, gy \right\rangle$$

$$+ \frac{\sigma}{[\rho]} \int_\Omega \sqrt{\left|\nabla \rho^n\right|^2 + \epsilon} \, dV.$$

Using Lemma 1 and canceling out $\frac{1}{2}\left\|M^{n+1}\right\|^2$, we obtain the desired inequality $E_\epsilon\left(M^{n+1}, \rho^{n+1}\right) \leq E_\epsilon\left(M^*, \rho^n\right)$.

$\square$

3   Spatial Discretization

In the previous section, we introduced a time discretization and proved that it is stable. A main ingredient in the proof of stability is the integration by parts at the continuous level. To implement the stability in the full discretization, we need to choose a proper spatial discretization that enables the integration by parts at the discrete level. A standard choice is to assume a rectangular domain Ω and use the Marker-And-Cell (MAC) space configuration, as shown in Figure 1. We proceed the discussion with the standard choice, but would like to note that the proposed time discretization can be combined with other spatial discretizations on which the integration by parts holds.

The density ρ is sampled at grid nodes, and its gradient is calculated at cell centers as:

$$(D_x \rho)_{i+\frac{1}{2}, j+\frac{1}{2}} = \frac{\rho_{i+1,j+1} + \rho_{i+1,j} - \rho_{i,j+1} - \rho_{ij}}{2\Delta x},$$

$$(D_y \rho)_{i+\frac{1}{2}, j+\frac{1}{2}} = \frac{\rho_{i+1,j+1} + \rho_{i,j+1} - \rho_{i+1,j} - \rho_{ij}}{2\Delta y},$$

$$\left.|\nabla \rho|\right|_{i+\frac{1}{2}, j+\frac{1}{2}} = \sqrt{(D_x \rho)^2_{i+\frac{1}{2}, j+\frac{1}{2}} + (D_y \rho)^2_{i+\frac{1}{2}, j+\frac{1}{2}}}.$$

As in [21], the curvature κ is then calculated at grid nodes as:

$$\kappa^{n+1}_{ij} = D_x \left[\frac{D_x \rho^{n+1}}{\sqrt{\left|\nabla \rho^n\right|^2 + \epsilon}} \right]_{ij} + D_y \left[\frac{D_y \rho^{n+1}}{\sqrt{\left|\nabla \rho^n\right|^2 + \epsilon}} \right]_{ij}.$$

Now, we present a full discretization of the semi-implicit time discretization (2)-(4). The full discretization of each component in $(m, n) \doteq M$ and $(u, v) \doteq \frac{M}{\sqrt{\rho}}$ is presented below. The density, ρ, on each cell face is averaged as $\rho_{i+\frac{1}{2}, j} = \frac{1}{2}\left(\rho_{ij} + \rho_{i+1,j}\right)$ and $\rho_{i,j+\frac{1}{2}} = \frac{1}{2}\left(\rho_{ij} + \rho_{i,j+1}\right)$.

$$\sqrt{\rho^n_{i+\frac{1}{2}, j}} \frac{m^{n+1}_{i+\frac{1}{2}, j} - m^n_{i+\frac{1}{2}, j}}{\Delta t} = -\frac{p^{n+1}_{i+1,j} - p^{n+1}_{ij}}{\Delta x} - \frac{\sigma}{[\rho]} \frac{\kappa^{n+1}_{ij} + \kappa^{n+1}_{i+1,j}}{2} \frac{\rho^n_{i+1,j} - \rho^n_{ij}}{\Delta x}$$

$$\sqrt{\rho^n_{i,j+\frac{1}{2}}} \frac{n^{n+1}_{i,j+\frac{1}{2}} - m^n_{i,j+\frac{1}{2}}}{\Delta t} = -\frac{p^{n+1}_{i,j+1} - p^{n+1}_{ij}}{\Delta y} - \frac{\sigma}{[\rho]} \frac{\kappa^{n+1}_{ij} + \kappa^{n+1}_{i,j+1}}{2} \frac{\rho^n_{i,j+1} - \rho^n_{ij}}{\Delta y} - \rho^n_{i,j+\frac{1}{2}} g$$

$$\frac{u^{n+1}_{i+\frac{1}{2}, j} - u^{n+1}_{i-\frac{1}{2}, j}}{\Delta x} + \frac{v^{n+1}_{i,j+\frac{1}{2}} - v^{n+1}_{i,j-\frac{1}{2}}}{\Delta y} = 0$$

$$\sqrt{\rho^n_{i,j+\frac{1}{2}}} \frac{n^{n+1}_{i,j+\frac{1}{2}} - m^n_{i,j+\frac{1}{2}}}{\Delta t} = -\frac{p^{n+1}_{i,j+1} - p^{n+1}_{ij}}{\Delta y} - \frac{\sigma}{[\rho]} \frac{\kappa^{n+1}_{ij} + \kappa^{n+1}_{i,j+1}}{2} \frac{\rho^n_{i,j+1} - \rho^n_{ij}}{\Delta y} - \rho^n_{i,j+\frac{1}{2}} g$$

$$\frac{\rho^{n+1}_{ij} - \rho^n_{ij}}{\Delta t} + \frac{1}{2}\left(u^{n+1}_{i+\frac{1}{2}, j} \frac{\rho^n_{i+1,j} - \rho^n_{ij}}{\Delta x} + u^{n+1}_{i-\frac{1}{2}, j} \frac{\rho^n_{ij} - \rho^n_{i-1,j}}{\Delta x} \right)$$

$$+ \frac{1}{2}\left(v^{n+1}_{i,j+\frac{1}{2}} \frac{\rho^n_{i,j+1} - \rho^n_{ij}}{\Delta y} + v^{n+1}_{i,j-\frac{1}{2}} \frac{\rho^n_{ij} - \rho^n_{i,j-1}}{\Delta x} \right) = 0$$

Figure 1: MAC configuration : domain Ω is the rectangle surrounded by the dotted line. Velocity field U is sampled on cell faces, so that $U \cdot e_1$ is sampled on each $\square$ and $U \cdot e_2$ on each $\triangle$. Pressure p, density ρ, and curvature κ are sampled on each $\bigcirc$.

For notational convenience, we denote the above full discretizations by:

$$\sqrt{\rho^n}\frac{M^{n+1} - M^*}{\Delta t} = -\nabla^h p^{n+1} - \rho^n ge_y - \frac{\sigma}{[\rho]}\kappa^{n+1}\nabla^h\rho^n \tag{5}$$

$$\nabla^h \cdot U^{n+1} = 0 \tag{6}$$

$$\frac{\rho^{n+1} - \rho^n}{\Delta t} + U^{n+1} \cdot \nabla^h\rho^n = 0 \tag{7}$$

The objective of this section is to prove that theorem 1 is still true with the full discretization. The analysis in the proof of the theorem has two components. One is for the time discretization, and the other is for the integration by parts. The time-related component is still valid, but the integration by parts, that appeared three times in the proof, need to be checked in this section.

Lemma 2. *(integration by parts at cell faces and cell centers) For any vector field U sampled at cell faces with $U = 0$ on $\partial\Omega$ and any scalar p at cell centers, we have*

$$\left\langle U, -\nabla^h p \right\rangle = \left\langle \nabla^h \cdot U, p \right\rangle$$

Proof.

6

$$\langle U, -\nabla^h p\rangle = -\sum_{i=1}^{isize-3}\sum_{j=1}^{jsize-2} u_{i+\frac{1}{2},j}\frac{p_{i+1,j}-p_{ij}}{\Delta x}\Delta x\Delta y - \sum_{i=1}^{isize-2}\sum_{j=1}^{jsize-3} v_{i,j+\frac{1}{2}}\frac{p_{i,j+1}-p_{ij}}{\Delta y}\Delta x\Delta y$$

$$= \sum_{i=1}^{isize-2}\sum_{j=1}^{jsize-2} p_{ij}\left(\frac{u_{i+\frac{1}{2},j}-u_{i-\frac{1}{2},j}}{\Delta x}+\frac{v_{i,j+\frac{1}{2}}-v_{i,j-\frac{1}{2}}}{\Delta y}\right)\Delta x\Delta y$$

$$+ \sum_{i=1}^{isize-2} -u_{isize-\frac{3}{2},j}\frac{p_{isize-2,j}}{\Delta x}\Delta x\Delta y + u_{\frac{1}{2},j}\frac{p_{ij}}{\Delta x}\Delta x\Delta y$$

$$+ \sum_{j=1}^{jsize-2} -v_{i,jsize-\frac{3}{2}}\frac{p_{i,jsize-2}}{\Delta y}\Delta x\Delta y + v_{i,\frac{1}{2}}\frac{p_{ij}}{\Delta y}\Delta x\Delta y$$

$$= \sum_{i=1}^{isize-2}\sum_{j=1}^{jsize-2} p_{ij}\left(\frac{u_{i+\frac{1}{2},j}-u_{i-\frac{1}{2},j}}{\Delta x}+\frac{v_{i,j+\frac{1}{2}}-v_{i,j-\frac{1}{2}}}{\Delta y}\right)\Delta x\Delta y + 0 + 0 = \left\langle \nabla^h\cdot U, p\right\rangle$$

$\square$

Lemma 3. *(integration by parts on cell centers and cell corners) For any vector field U sampled on cell corners with $U=0$ on $\partial\Omega$ and any scalar p on cell centers, we have*

$$\left\langle \nabla^h\cdot U, p\right\rangle = \left\langle U, -\nabla^h p\right\rangle$$

Proof.

$$\langle u, D_x p\rangle = \sum_{i=1}^{isize-3}\sum_{j=1}^{jsize-3} u_{i+\frac{1}{2},j+\frac{1}{2}}\frac{p_{i+1,j+1}+p_{i+1,j+1}-p_{i,j+1}-p_{ij}}{2\Delta x}\Delta x\Delta y$$

$$= \sum_{i=2}^{isize-2}\sum_{j=2}^{jsize-2} u_{i-\frac{1}{2},j-\frac{1}{2}}\frac{p_{ij}}{2\Delta x} + \sum_{i=2}^{isize-2}\sum_{j=1}^{jsize-3} u_{i-\frac{1}{2},j+\frac{1}{2}}\frac{p_{ij}}{2\Delta x}$$

$$- \sum_{i=1}^{isize-3}\sum_{j=2}^{jsize-2} u_{i+\frac{1}{2},j-\frac{1}{2}}\frac{p_{ij}}{2\Delta x} - \sum_{i=1}^{isize-3}\sum_{j=1}^{jsize-3} u_{i-\frac{1}{2},j-\frac{1}{2}}\frac{p_{ij}}{2\Delta x}$$

Using the assumption $u=0$ on $\partial\Omega$, the four sums are combined as:

$$\langle u, D_x p\rangle = -\sum_{i=1}^{isize-2}\sum_{j=1}^{jsize-2}\frac{u_{i-\frac{1}{2},j-\frac{1}{2}}+u_{i-\frac{1}{2},j+\frac{1}{2}}-u_{i+\frac{1}{2},j-\frac{1}{2}}-u_{i+\frac{1}{2},j+\frac{1}{2}}}{2\Delta x}p_{ij}$$

$$= -\left\langle D_x u, p\right\rangle$$

Similarly, $\langle v, D_y p\rangle = \langle -D_y v, p\rangle$. $\square$

Theorem 2. *(Unconditional stability of the full discretization) Let (M^{n+1},ρ^{n+1}) be generated from (M^*,ρ^*) by (5)-(7), and M^* be generated from M^n and $U^{n+\frac{1}{2}}$ by (1) and [11]. For any $\Delta t > 0$ and $\epsilon > 0$, we have:*

$$E_\epsilon(M^{n+1},\rho^{n+1}) \le E_\epsilon(M^n,\rho^n)$$

Proof. We basically repeat the proof of theorem 1 using the previous lemmas whenever integration by parts is evoked.

$$\left\langle M^{n+1}, \frac{M^{n+1}-M^*}{\Delta t}\right\rangle = \left\langle U^{n+1}, -\nabla^h p^{n+1}-\rho^n g\nabla^h y - \frac{\sigma}{[\rho]}\kappa^{n+1}\nabla^h\rho^n\right\rangle$$

$$= 0 + \left\langle \nabla^h\cdot\left(U^{n+1}\rho^n\right), gy\right\rangle - \frac{\sigma}{[\rho]}\left\langle U^{n+1}\cdot\nabla^h\rho^n, \frac{\sigma}{[\rho]}\kappa^{n+1}\right\rangle, \text{ by Lemma 2}$$

$$= -\left\langle \frac{\rho^{n+1}-\rho^n}{\Delta t}, gy\right\rangle - \frac{\sigma}{[\rho]}\left\langle \frac{\rho^{n+1}-\rho^n}{\Delta t}, \kappa^{n+1}\right\rangle$$

With the non-slip boundary condition on $\partial\Omega$, $\left(\rho^{n+1} - \rho^n\right)/\Delta t = 0$ on $\partial\Omega$, and the following integration by parts holds;

$$\left\langle \frac{\rho^{n+1} - \rho^n}{\Delta t}, \nabla^h \cdot \left(\frac{\nabla^h \rho^{n+1}}{\sqrt{|\nabla^h \rho^n|^2 + \epsilon}}\right)\right\rangle = -\left\langle \frac{\nabla^h \rho^{n+1} - \nabla^h \rho^n}{\Delta t}, \frac{\nabla^h \rho^{n+1}}{\sqrt{|\nabla^h \rho^n|^2 + \epsilon}}\right\rangle, \, by \, Lemma \, 3$$

$$= \int_\Omega \frac{-|\nabla^h \rho^{n+1}|^2 + \nabla^h \rho^n \cdot \nabla^h \rho^{n+1}}{\Delta t \sqrt{|\nabla^h \rho^n|^2 + \epsilon}} dV$$

Using the following two basic inequalities, we obtain:

$$\left\langle M^{n+1}, \frac{M^{n+1} - M^*}{\Delta t}\right\rangle \le -\left\langle \frac{\rho^{n+1} - \rho^n}{\Delta t}, gy\right\rangle + \frac{\sigma}{[\rho]} \int_\Omega \frac{\sqrt{|\nabla^h \rho^n|^2 + \epsilon} - \sqrt{|\nabla^h \rho^{n+1}|^2 + \epsilon}}{\Delta t} dV$$

$$\left\|M^{n+1}\right\|^2 + \left\langle \rho^{n+1}, gy\right\rangle + \frac{\sigma}{[\rho]} \int_\Omega \sqrt{|\nabla^h \rho^{n+1}|^2 + \epsilon} dV \le \left\langle M^{n+1}, M^*\right\rangle + \left\langle \rho^n, gy\right\rangle + \frac{\sigma}{[\rho]} \int_\Omega \sqrt{|\nabla^h \rho^n|^2 + \epsilon} dV$$

$$\le \frac{1}{2}\left\|M^{n+1}\right\|^2 + \frac{1}{2}\left\|M^*\right\|^2 + \left\langle \rho^n, gy\right\rangle$$

$$+ \frac{\sigma}{[\rho]} \int_\Omega \sqrt{|\nabla^h \rho^n|^2 + \epsilon} dV$$

Using Lemma 1 and cancelling out $\frac{1}{2}\left\|M^{n+1}\right\|^2$, we obtain the desired inequality $E_\epsilon\left(M^{n+1}, \rho^{n+1}\right) \le E_\epsilon\left(M^*, \rho^n\right)$. $\square$

4   Numerical Experiments

In this section, we solve a benchmark problem with the proposed approximations. We first show that the numerical results confirm the analysis of section 2 and 3, and then we report some drawbacks that the approximation exhibit in practice. All the linear systems are solved by GMRES with stopping criteria $\|r^n\| \le \|r^0\| \times 10^{-7}$, and the parameter ϵ is chosen to be Δx. The numerical computation were performed on a personal computer with a 3.60 GHz CPU and 16.0 GB memory.

4.1   Example 1 : Bubble rising

As a benchmark, the bubble rising set up [21, 10, 18] is taken to validate the two stability analyses. One is $\|M^*\|_{L^2} = \|M^n\|_{L^2}$ in lemma 1, and the other is $E_\epsilon\left(M^{n+1}, \rho^{n+1}\right) \le E_\epsilon\left(M^n, \rho^n\right)$ in theorem 2.

The problem initially places a circular bubble centered at $(0,0)$ with radius $R = 1/3$ in a domain $\Omega = [-1,1] \times [-1,2]$. Due to the gravity acceleration $g = 9.8$ and the density differences between $\rho_b = 1$ and $\rho_c = 2$, the bubble rises with a deformation on its shape. A Bond number of $Bo = \frac{4g\rho_c R^2}{\sigma} = 300$ is used to set the coefficient σ. Based on the CFL analysis by Brackbill et al. [4], the usual CFL condition was suggested in Boundary Condition Capturing Method (BCCM) by Kang et al. [10] as follows:

$$C_{CFL} = \frac{\|u\|_\infty}{\Delta x} + \frac{\|v\|_\infty}{\Delta y}$$

$$G_{CFL} = \frac{4|g|}{\Delta y}$$

$$S_{CFL} = \sqrt{\frac{\sigma}{\rho_b \left[\min\left(\Delta x, \Delta y\right)\right]^3}}$$

$$CFL = \frac{\Delta t}{2} \cdot \left(C_{CFL} + \sqrt{C_{CFL}^2 + 4G_{CFL}^2 + 4S_{CFL}^2}\right)$$

Compared to the CFL= 2 in BCCM, our approximation may take a CFL of 20, CFL= 40, or any larger number while preserving the energy stability. Figure 2 validates the stability: the total energy $E_\epsilon\left(M^n, \rho^n\right)$ is monotonically decreasing. Furthermore, figure ?? validates the conservation of the L^2 norm in the convection solver within machine epsilon.

Figure 4 shows that our results are comparable with the conventional result of BCCM even though there is a big difference in CFL numbers. As the grid is refined, our numerical results are convergent, as presented in figure 5.
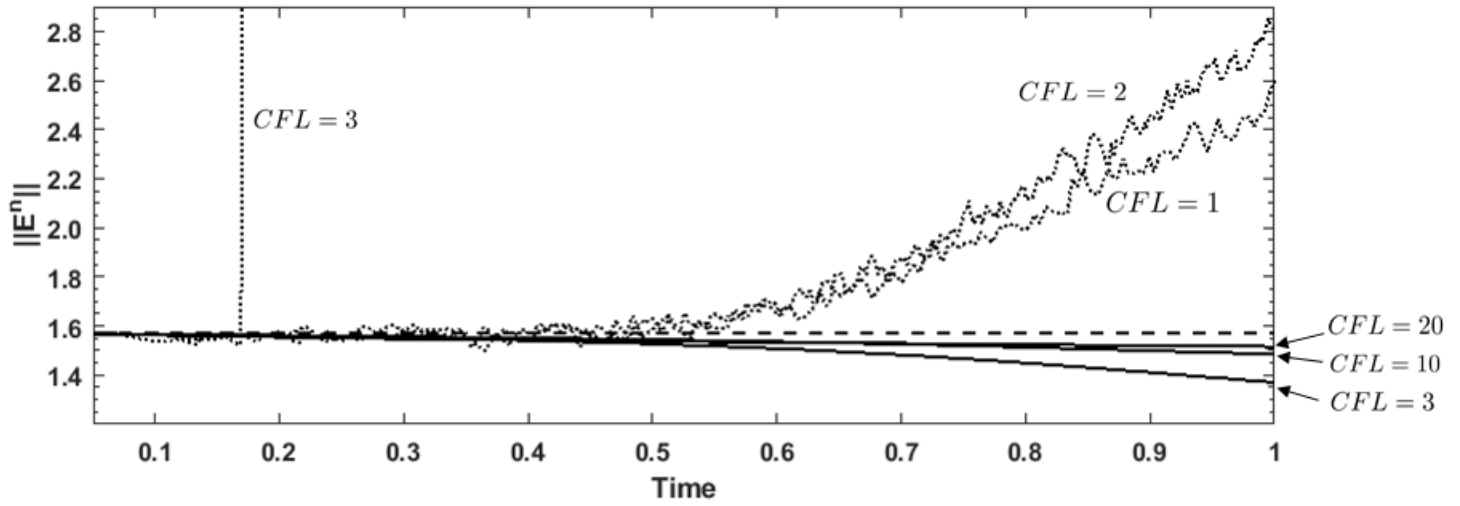
Figure 2: the temporal changes of the total energy are compared between BCCM(:) and the current work (–) in the bubble rising problem with $h = 1/40$ and various CFL conditions. Unlike BCCM [10], the energy of our approximation monotonically decreases, which validates theorem 2.
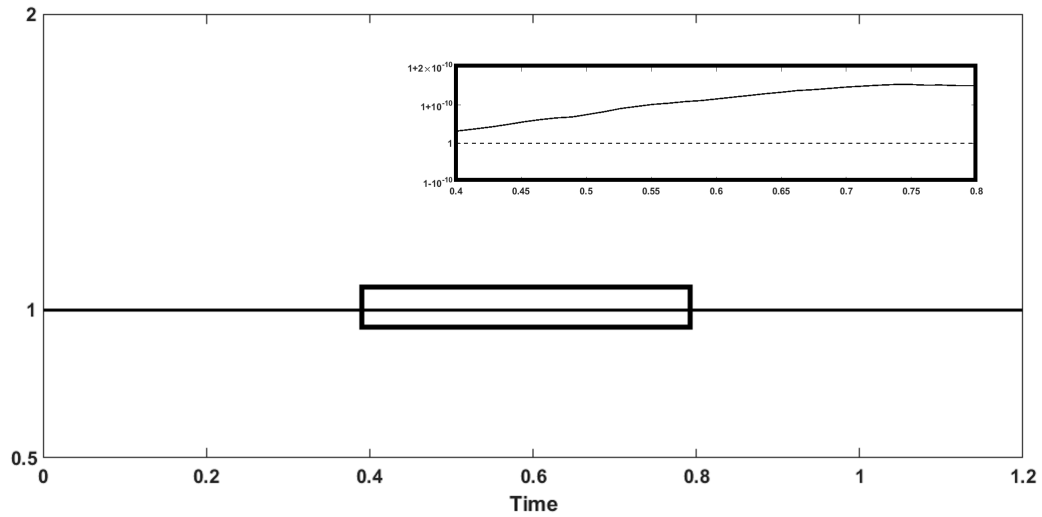
Figure 3: Ratio $\|M^*\|_{L^2} / \|M^n\|_{L^2}$ in the bubble rising problem with $h = 1/40$ and CFL= 20. Confirming lemma 1, the ratio is 1 within machine epsilon. The inset magnifies the region time= $[0.4, 0.8]$.
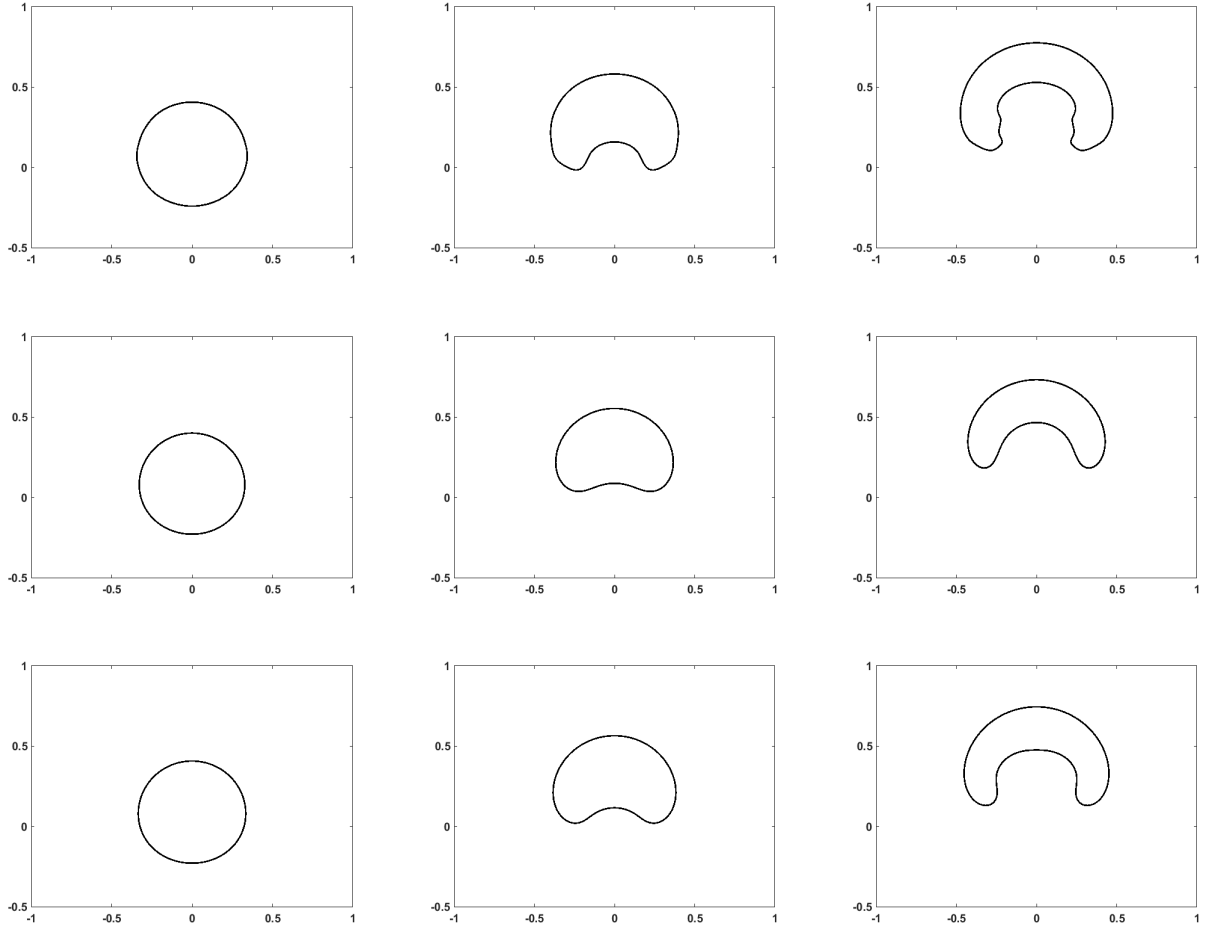
Figure 4: Numerical results of bubble rising with $h = 1/80$: the top line is the results of BCCM with CFL= 2, the middle and bottom are the results of the current work with CFL=10 and CFL= 20, respectively. The elapsed times are $t = 0.25$ (left), 0.5 (middle), and 0.75 (right).
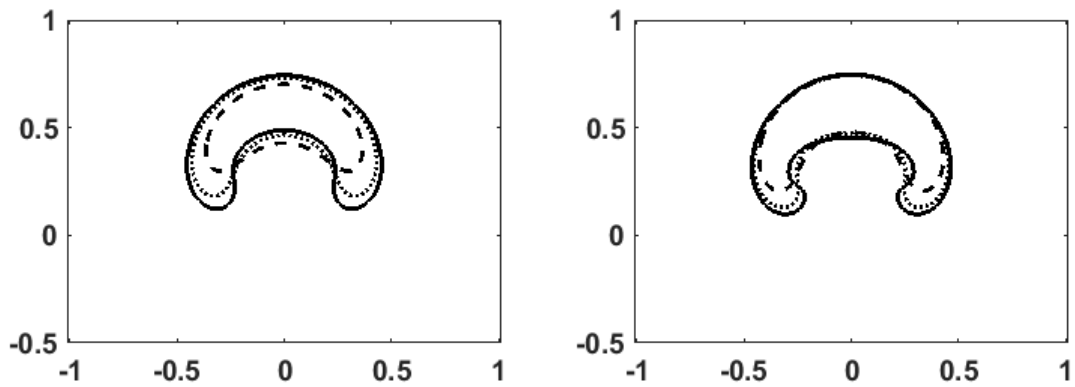
Figure 5: convergence study with $h = 1/160$ (−), $1/80$ (:), and $1/40$ (- -) are compared. In either case of CFL= 10 (left) or 20 (right), the results show convergence.
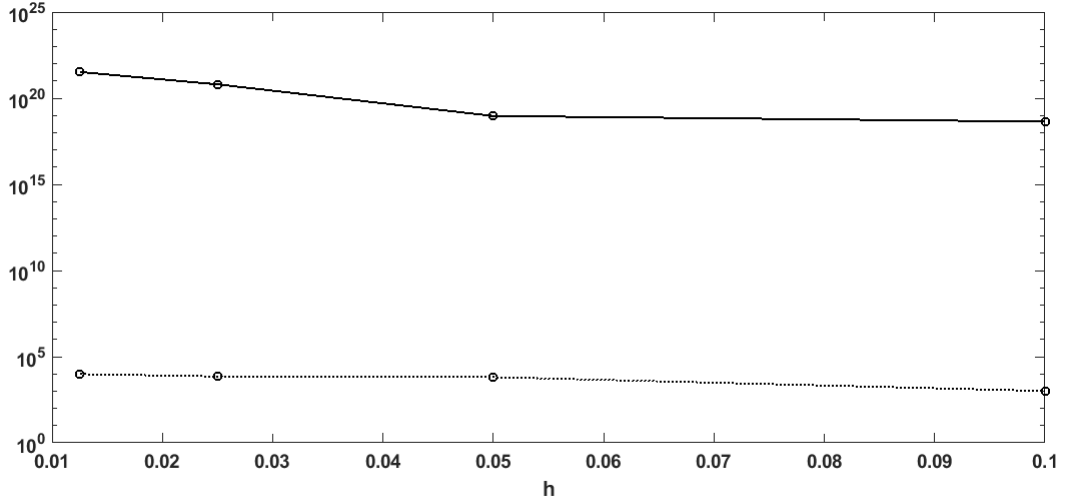
Figure 6: The condition numbers of the linear systems are compared between ours (−) and BCCM (:) in the bubble rising problem with $h = 1/40$ and CFL= 20.

4.2 Drawbacks in practice

The previous section confirmed that our approximation can take much larger time steps than the conventional method. However, the unconditional stability comes at the expense of a large condition number. The linear system associated with our approximation is given below.

$$\begin{bmatrix} I & \Delta t \left(\sigma \nabla \cdot \left(\frac{\cdot}{|\nabla \rho^n|} \right) \nabla \rho^n \right) & \frac{\Delta t}{\sqrt{\rho^n}} \nabla \\ O & I & O \\ \nabla \cdot \left(\frac{\cdot}{\sqrt{\rho^n}} \right) & O & O \end{bmatrix} \begin{bmatrix} M^{n+1} \\ \rho^{n+1} \\ p^{n+1} \end{bmatrix} = \begin{bmatrix} M^* \\ \left(I - \Delta t \frac{M^{n+1}}{\sqrt{\rho^n}} \cdot \nabla \right) \rho^n \\ O \end{bmatrix}$$

The jump discontinuity in ρ^n makes $1/|\nabla \rho^n|$ very large, and the matrix becomes highly ill-conditioned, as shown in figure 6. GMRES requires more memory as the iteration number increases, and the restarted GMRES(m) has been used in practice. Figure 7 shows that the restarted GMRES is not appropriate for the ill-conditioned matrix. Thus we solve the linear system by GMRES without restarting.

In BCCM, the interface is represented by a level set function, and the transition width of the density across the interface is kept to be consistent through the level set reinitialization. Our aim in this study is to devise a stable method. At this moment, we do not know any reinitialization approach that may result in energy stability. Without reinitialization, the transition width becomes nonuniform as the simulation proceeds. Figure 8 shows that BCCM keeps the narrow and uniform bandwidth, agreeing well with the physical experiment of [3], but ours does not.

5 Discussion and conclusion

We introduced a semi-implicit approximation for simulating two-phase fluids with surface tension, and provided a mathematical analysis that the approximation is unconditionally stable in the sense that the total energy does not increase for any time step. Numerical results confirmed the unconditional stability, but also pointed to two practical drawbacks. One is that the associated linear system is very ill-conditioned, which will require the design of an efficient preconditioners. The other is that the transition of the density between the two phases is not controlled during the simulation. We leave the resolution of those issues to future work.
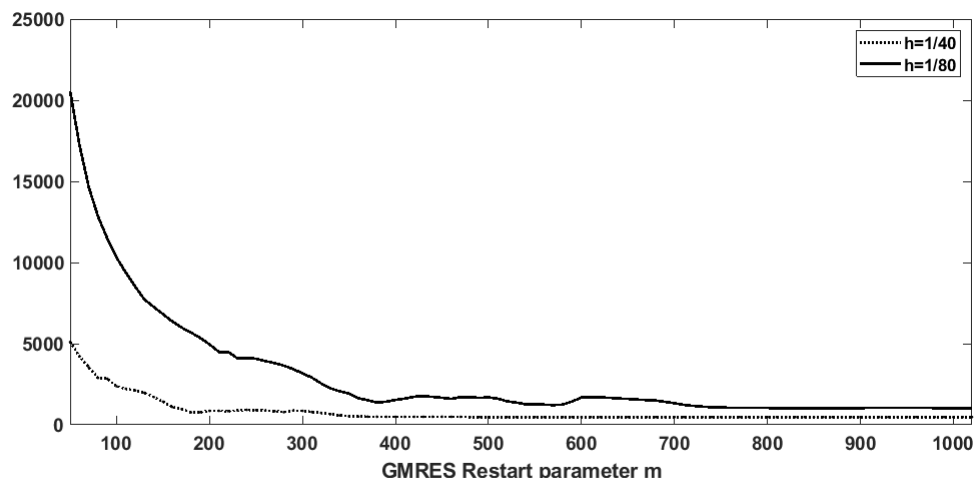
Figure 7: The iteration number necessary for the restarted GMRES(m) to converge in the bubble rising problem with CFL= 40.

Acknowledgement

References

[1] V. E. Badalassi, H. D. Ceniceros, and S. Banerjee. Computation of multiphase systems with phase field models. *J. Comput. Phys.*, 190(2):371–397, 2003.

[2] J. B. Bell, P. Colella, and H. M. Glaz. A second-order projection method for the incompressible navier-stokes equations. *J. Comput. Phys.*, 85(2):257–283, 1989.

[3] D. Bhaga and M. E. Weber. Bubbles in viscous liquids: shapes, wakes and velocities. *J. Fluid Mech.*, 105:61–85, 1981.

[4] J. U. Brackbill, D. B. Kothe, and C. Zemach. A continuum method for modeling surface tension. *J. Comput. Phys.*, 100(2):335–354, 1992.

[5] D. Brown, R. Cortez, and M. Minion. Accurate projection methods for the incompressible navier–stokes equations. *J. Comput. Phys.*, 168(2):464–499, 2001.

[6] Y. C. Chang, T. Hou, B. Merriman, and S. Osher. Eulerian capturing methods based on a level set formulation for incompressible fluid interfaces. *J. Comput. Phys.*, 124(449-464):18, 1996.

[7] S. Hysing. A new implicit surface tension implementation for interfacial flows. *Int. J. Numer. Methods in Fluids*, 51(6):659–672, 2006.

[8] D. Jamet, D. Torres, and J. U. Brackbill. On the theory and computation of surface tension: the elimination of parasitic currents through energy conservation in the saecond-gradient method. *J. Comput. Phys.*, 182:262–276, 2002.

[9] A. Jarauta, P. Ryzhakov, J. Pons-Prats, and M. Secanell. An implicit surface tension model for the analysis of droplet dynamics. *J. Comput. Phys.*, 374:1196 − 1218, 2018.
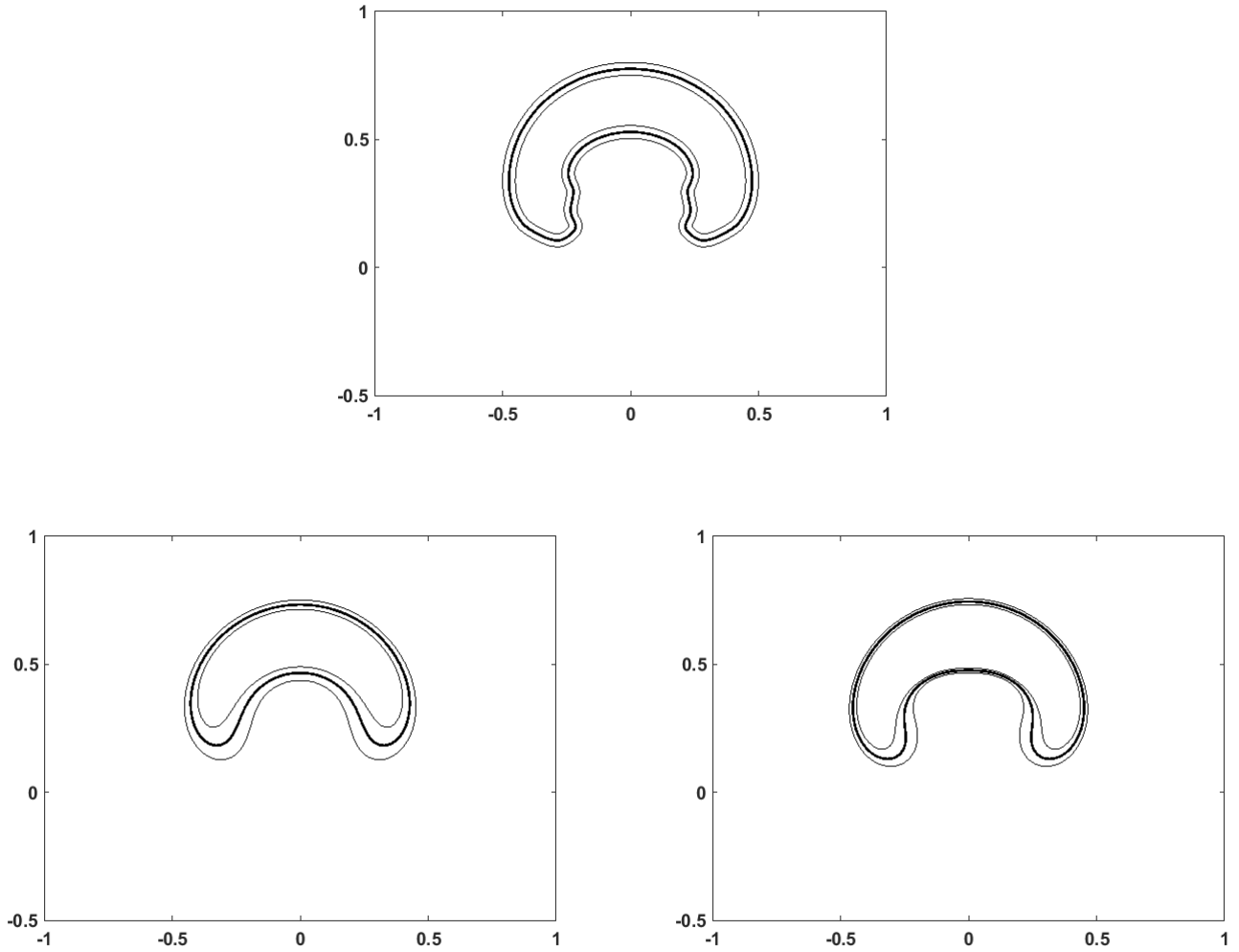
Figure 8: the transition region of density at $t = 0.75$ and $h = 1/80$: BCCM with CFL= 2 (top), ours with CFL= 10 (bottom left) and 20 (bottom right).

[10] M. Kang, R. Fedkiw, and X. D. Liu. A Boundary Condition Capturing Method for Multiphase Incompressible Flow. *J. Sci. Comput.*, 15:323–360, 2000.

[11] J. Kim, J. Jung, Y. Park, C. Min, and B. Lee. An energy-stable and second-order accurate method for solving the incompressible navier-stokes equations. *J. Korean Soc. Ind. Appl. Math.*, 23(2):93–114, 2019.

[12] J. Kim and P. Moin. Application of a Fractional-step Method to Incompressible Navier-Stokes Equations. *J. Comput. Phys.*, 59:308–323, 1985.

[13] B. Lee and C. Min. An energy-stable method for solving the incompressible navier-stokes equations with non-slip boundary condition. *J. Comput. Phys.*, 360:104 − 119, 2018.

[14] K. Nikitin, M. Olshanskii, K. Terekhov, and Y. Vassilevski. A splitting method for numerical simulation of free surface flows of incompressible fluids with surface tension. *Comput. Methods Appl. Math.*, 15:59–78, 2015.

[15] A. A. Novotny and J. Sokolowski. Topological derivatives in shape optimization. *Interaction of Mechanics and Mathematics, Springer*, 2013.

[16] S. Popinet. An accurate adaptive solver for surface-tension-driven interfacial flows. *J. Comput. Phys.*, 228:5838–5866, 2009.

[17] C. Pozrikidis. Introduction to theoretical and computational fluid dynamics. *Oxford university press*, 1997.

[18] M. Sussman, E. Fatemi, P. Smereka, and S. Osher. An Improved Level Set Method for Incompressible Two-Phase Flows. *Computers and Fluids*, 27:663–680, 1998.

[19] M. Sussman and M. Ohta. A stable and efficient method for treating surface tension in incompressible two-phase flow. *SIAM J. Sci. Comput.*, 31:2447–2471, 2009.

[20] M. Sussman and E. G. Puckett. A coupled level set and volume-of-vluid method for computing 3d and axisymmetric incompressible two-phase flows. *J. Comput. Phys.*, 162:301–337, 2000.

[21] M. Sussman, P. Smereka, and S. Osher. A Level Set Approach for Computing Solutions to Incompressible Two-Phase Flow. *J. Comput. Phys.*, 114:146–159, 1994.

[22] W. Zheng, B. Zhu, B. Kim, and R. Fedkiw. A new incompressibility discretization for a hybrid particle mac grid representation with surface tension. *J. Comput. Phys.*, 280:96–142, 2015.